TKK Dissertations 217
Espoo 2010

AEROSOL SYNTHESIS OF CARBON NANOTUBES AND NANOBUDS

Doctoral Dissertation

Anton Anisimov

Aalto University
School of Science and Technology
Faculty of Information and Natural Sciences
Department of Applied Physics

TKK Dissertations 217
Espoo 2010

AEROSOL SYNTHESIS OF CARBON NANOTUBES AND NANOBUDS

Doctoral Dissertation

Anton Anisimov

Doctoral dissertation for the degree of Doctor of Science in Technology to be presented with due permission of the Faculty of Information and Natural Sciences for public examination and debate in Auditorium U154 at the Aalto University School of Science and Technology (Espoo, Finland) on the 9th of April 2010 at 12 noon.

Aalto University
School of Science and Technology
Faculty of Information and Natural Sciences
Department of Applied Physics

Aalto-yliopisto
Teknillinen korkeakoulu
Informaatio- ja luonnontieteiden tiedekunta
Teknillisen fysiikan laitos

Distribution:
Aalto University
School of Science and Technology
Faculty of Information and Natural Sciences
Department of Applied Physics
P.O. Box 11100
FI - 00076 Aalto
FINLAND
URL: http://tfy.tkk.fi/
Tel. +358-9-470 23153
Fax +358-9-470 23155
E-mail: anton.anisimov@tkk.fi

ISBN 978-952-60-3086-9
ISBN 978-952-60-3087-6 (PDF)
ISSN 1795-2239
ISSN 1795-4584 (PDF)
URL: http://lib.tkk.fi/Diss/2010/isbn9789526030876/

TKK-DISS-2740

Multiprint Oy
Espoo 2010

Aalto University

ABSTRACT OF DOCTORAL DISSERTATION	AALTO UNIVERSITY SCHOOL OF SCIENCE AND TECHNOLOGY P.O. BOX 11000, FI-00076 AALTO http://www.aalto.fi

Author Anton Anisimov

Name of the dissertation
Aerosol synthesis of carbon nanotubes and nanobuds

Manuscript submitted 15.12.2009	Manuscript revised 12.03.2010
Date of the defence 09.04.2010	
☐ Monograph	☒ Article dissertation (summary + original articles)

Faculty	Faculty of Information and Natural Sciences
Department	Department of Applied Physics
Field of research	Nanotechnology
Opponent(s)	Professor Yoshikazu Homma
Supervisor	Professor Esko I. Kauppinen
Instructor	Docent Albert G. Nasibulin

Abstract

This thesis presents the results of experimental investigations of single-walled carbon nanotube (SWCNT) and nanobud synthesis. These carbon nanomaterials were synthesized by two different methods based on CO disproportionation on the surface of iron particles produced by hot-wire generator and ferrocene decomposition methods.

Studies of CO disproportionation in the presence of etching molecules (H_2O and CO_2) led to the discovery of a novel hybrid carbon material — SWCNTs covered by covalently bonded fullerenes — carbon nanobuds. The reagent concentrations required for nanobud synthesis were found to be between 45 and 245 ppm for H_2O and between 2000 and 6000 ppm for CO_2. The growth mechanism of the nanobuds and their properties were examined.

On the basis of *in situ* sampling investigations, the kinetics of the SWCNT growth was studied. For temperatures of 804, 836, 851, and 915 °C, the average growth rates were found to be 0.67, 1.11, 1.01, and 2.70 μm/s, respectively. It was found that the growth rate constant complies with the Arrhenius dependence with an activation energy of E_a = 1.39 eV, which can be attributed to the diffusion of carbon atoms in the solid iron catalyst.

A new method for separating bundles and individual SWCNTs is proposed. This method is based on the fact that bundled SWCNTs coming from the reactor are charged, while individual SWCNTs remain electrically neutral. Studies of the charging phenomenon revealed that SWCNT bundles were charged (up to 99%) and could carry up to 5 elementary charges. It is proposed that SWCNT bundles were positively charged due to electron emissions and negatively charged due to the emission of impurities from the surface.

As a potential SWCNT application, a simple and direct thermo-compression method for integrating SWCNT films with adjustable thicknesses, transparency, and conductivity into polymer films is demonstrated. The produced SWCNT/polyethylene composite films exhibited good optical transparency and conductivity as well as high mechanical flexibility. SWCNT/polyethylene thin films demonstrated excellent cold electron field emission properties.

Keywords carbon nanotube, carbon nanobud, synthesis, etching, mechanism, charging phenomena, field emission

ISBN (printed)	978-952-60-3086-9	ISSN (printed)	1795-2239
ISBN (pdf)	978-952-60-3087-6	ISSN (pdf)	1795-4584
Language	English	Number of pages	48 p. + app. 60 p.
Publisher	Aalto University School of Science and Technology		
Print distribution	Department of Applied Physics, Aalto University School of Science and Technology		

☒ The dissertation can be read at http://lib.tkk.fi/Diss/2010/isbn9789526030876/

Preface

The research work for the present thesis was carried out at the Nanomaterials Group of Department of Applied Physics at Helsinki University of Technology (TKK), during the years 2006-2009.

My sincere thanks go to Professor Esko I. Kauppinen for offering me the possibility to work in his group and to make my dissertation. His scientific expertise and the demanding environment of his group were a constant challenge during all stages of the work.

I am especially grateful to Dr. Albert G. Nasibulin, docent at the Department of Applied Physics at TKK, for the innumerable fruitful discussions and his invaluable support.

My warmest thanks go to Dr. Sergey D. Shandakov, who has been my mentor for many years, both during my work on M.Sc. thesis in Russia and afterwards, when we were both working at the Nanomaterials Group in Finland.

I am indebted to all my co-authors especially Dr. H. Jiang, Dr. D. P. Brown, Dr. D. Gonzalez, Dr. P. Queipo, Dr. P. V. Pikhitsa, Dr. P. Launois, J. Cambedouzou, Dr. A. V. Krasheninnikov, Dr. A. Moisala, Dr. A. Hassanien, Prof. D.E. Resasco, Prof. D. Tománek, Dr. M. Pudas, Prof. J. Ruokolainen, A. Ollikainen.

I also would like to thank the whole personnel of the Nanomaterials Group, especially Dr. Janne Raula, Dr. Ilya Anoshkin, Prasantha Mudimela, Ying Tian, Marina Zavodchikova, Larisa Nasibulina, Simas Rackauskas, Antti Kaskela, for creating a very friendly working environment.

Furthermore, I would like to thank the pre-examiners of my thesis, Professor Jorma Jokiniemi, and Dr. Jyrki Mäkelä for valuable feedback and constructive comments.

This study was financially supported by TEKES, Nokia Oy, Canatu Oy and by the CNB-E project of the Aalto University MIDE program.

Finally, I am also very grateful to all of my family members and my friends in Russia for loving me always.

Contents

List of Publications

I **Anisimov, A.S.**, Nasibulin, A.G., Jiang, H., Launois, P., Cambedouzou, J., Shandakov, S.D., Kauppinen, E.I., 2010. Mechanistic investigations of single-walled carbon nanotube synthesis by ferrocene vapour decomposition in carbon monoxide. *Carbon*, 48, 380–388.

II Nasibulin, A.G., Brown, D.P., Queipo, P., Gonzalez, D., Jiang, H., **Anisimov, A.S.**, Kauppinen, E.I., 2006. Effect of CO_2 and H_2O on the synthesis of single-walled CNTs. *Phys. Stat. Sol.*, 243, 3087–3090.

III Nasibulin, A.G., Pikhitsa, P.V., Jiang, H., Brown, D.P., Krasheninnikov, A.V., **Anisimov, A.S.**, Queipo, P., Moisala, A., Gonzalez, D., Lientschnig, G., Hassanien, A., Shandakov, S.D., Lolli, G., Resasco, D.E., Choi, M., Tománek, D., Kauppinen E.I., 2007. A novel hybrid carbon nanomaterial. *Nat. Nanotechnol*., 2, 156–161.

IV Nasibulin, A.G., **Anisimov, A.S.**, Pikhitsa, P.V., Jiang, H., Brown, D.P., Choi, M., Kauppinen, E.I., 2007. Investigations of nanobud formation. *Chem. Phys. Lett*., 446, 109–114.

V Gonzalez, D., Nasibulin, A.G., Shandakov, S.D., Jiang, H., Queipo, P., **Anisimov, A.S.**, Tsuneta, T., Kauppinen E.I., 2006. Spontaneous charging of single-walled carbon nanotubes: a novel method for the selective substrate deposition of individual tubes at ambient temperature. *Chem. Mater*., 18, 5052–5057.

VI Nasibulin, A.G., Shandakov, S.D., **Anisimov, A.S.**, Gonzalez, D., Jiang, H., Pudas, M., Queipo, P., Kauppinen, E.I., 2008. Charging of aerosol products during ferrocene vapour decomposition in N_2 and CO atmospheres. *J. Chem. Phys.*, 112, 5762–5769.

VII Nasibulin, A.G., Ollikainen, A., **Anisimov, A.S.**, Brown, D.P., Pikhitsa, P.V., Holopainen, S., Penttilä, J.S., Helistö, P., Ruokolainen, J., Choi, M., Kauppinen, E.I., 2008. Integration of single-walled carbon nanotubes into polymer films by thermo-compression, *Chem. Eng. J.*, 136, 409–413.

Author contribution

I: The author is mainly responsible for all parts of this work and co-writing the paper (contribution of 80%).

II: The author contributed to SWCNT synthesis, sample preparation, DMA measurements, and analyzing the results (contribution of 30%).

III: The author contributed to SWCNT and nanobud synthesis and optimizing the synthesis conditions, and sample preparation (contribution of 30%).

IV: The author contributed to SWCNT and nanobud synthesis and optimizing the synthesis conditions, and sample preparation (contribution of 45%).

V: The author contributed to SWCNT synthesis, sample preparation, DMA measurements, and analyzing the results (contribution of 30%).

VI: The author contributed to SWCNT synthesis, sample preparation, DMA measurements, analyzing the results, and co-writing the paper (contribution of 40%).

VII: The author contributed to SWCNT synthesis, sample preparation, analyzing the results, SEM imaging, analyzing the results, and co-writing the paper (contribution of 40%).

List of Abbreviations and Symbols

L	length
au	arbitrary unit
amu	atomic mass unit
p	partial pressure
T	temperature
t_{RES}	residence time
Q	flow rate (gas compound indicated as a subscript)
σ	geometric standard deviation
SWCNT	single-walled carbon nanotube
CVD	chemical vapour deposition
CPC	condensation particle counter
DMA	differential mobility analyzer
HWG	hot-wire generator
NSD	number size distribution
TEM	transmission electron microscopy/transmission electron microscope
LDI-TOF	laser desorption ionization time-of-flight spectrometry
ESP	electrostatic precipitator (for aerosol particle deposition on a TEM grid)
ESF	electrostatic filter (for collection of charged aerosol particles)

1 Introduction

Carbon nanotubes (CNTs) are molecular-scale tubes of graphitic carbon. Intensive research into CNTs was initiated in 1991 by Prof. Sumio Iijima after his landmark publication [1], in which he showed clear structures of double-walled and multiwalled CNTs. Single-walled CNTs (SWCNT) were independently discovered by Iijima and Ichihashi [2] and Bethune *et al.* [3] in 1993. SWCNTs have diameters of the order of single nanometers, with a tube length that can be many millions of times longer.

Widespread interest in CNTs soon stemmed from their diverse useful properties, which can provide various applications in many fields, such as field electron emission technologies, nanoelectronics, superstrong fibres, composite materials, catalysts, molecular wires, switches, and photonic materials, etc.

The most common CNT synthesis methods are arc-discharge, laser ablation, and chemical vapour deposition (CVD). Arc-discharge and laser ablation methods are based on vaporization of solid carbon targets. The advantage of these methods is the high crystallinity of the CNT sample, i.e. the low number of defects in the CNT wall structure [1,4]. Nevertheless, these methods generally produce a complex mixture of SWCNTs or multiwalled CNTs (MWCNTs), metal particles, carbon particles, and amorphous carbon, making purification a necessary process step.

The CVD method involves decomposition of carbon-containing precursor molecules on the surface of transition metal catalyst particles, typically Fe, Ni and Co, usually supported on a substrate. Recently, it was demonstrated that even such materials as Au, Ag, Cu, Al_2O_3 and diamond [5-7] can act as a catalyst for SWCNT synthesis. Alternatively, catalytic CNT synthesis can be performed in the gas phase without a support material. Unsupported CVD methods have many advantages over other methods. The CVD methods are operated at essentially low temperatures (about 600–1000 °C) and allow continuous CNT production. From an industrial point of view, for many applications it is desirable to produce and/or directly deposit CNTs onto the required substrates, so that time-consuming steps of CNT purification from the catalyst and support, and dispersion and deposition processes are avoided. Therefore, the aerosol

unsupported CVD technique, which allows the production of high-quality clean SWCNTs, is preferable. Also, the amount of the undesirable products can be decreased by utilizing CO as a carbon source, which is known to disintegrate only on the surface of catalyst. An additional advantage of the aerosol unsupported method is the possibility of studying the mechanism and kinetics of SWCNT formation by means of on-line aerosol measurements and *in situ* sampling experiments.

This thesis presents studies of SWCNT aerosol synthesis in a hot-wire generator reactor [8] and in a reactor based on ferrocene vapour decomposition [9]. The aim of these studies has been to better understand the mechanism and kinetics of SWCNT growth. Optimization of synthesis parameters, such as temperature and gas composition, has enabled the synthesis of a novel hybrid material that combines fullerenes and SWCNTs into single structure — carbon nanobuds. Randomly oriented mats of nanobuds have been found to show excellent field-emission properties. This thesis introduces novel methods for the separation of bundled and individual SWCNTs and for the integration of SWCNT mats into polymers.

This work is based on publications I–VII, which are attached as appendices. On the basis of *in situ* sampling from different locations in the reactor, the kinetics of SWCNT growth was studied in Paper I. The essential role of etching molecules (CO_2 and H_2O) in the CNT formation was demonstrated in Paper II. The synthesis of a novel hybrid material, nanobuds, that combines fullerenes and SWCNTs in a single structure in which the fullerenes are covalently bonded to the outer surface of the SWCNTs, was shown for the first time in Paper III. The mechanism of nanobud formation was discussed in Paper IV. On the basis of the observed CNT self-charging phenomena, a novel method for the gas-phase separation of individual CNTs from bundles and their subsequent deposition onto any substrate at ambient temperature was introduced in Paper V. The charging phenomenon of CNTs was thoroughly investigated in Paper VI. As one of the applications of SWCNTs, a simple and efficient one-step integration process for transferring SWCNT mats into polyethylene (PE) thin films was demonstrated in Paper VII.

2 Literature review

2.1 Carbon nanotubes (structure, properties, and applications)

A CNT can be thought of as a graphene sheet rolled up to form a cylinder [10,11]. CNTs may be found either as individual cylinders, i.e. SWCNTs, or as two or more concentric cylinders, i.e. MWCNTs (Figure 1).

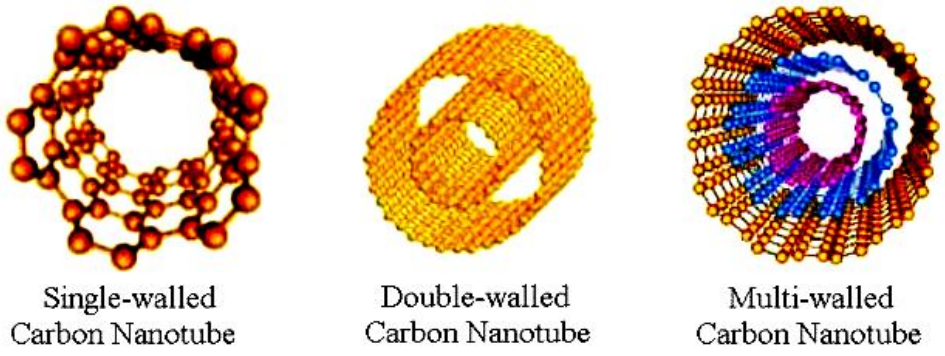

Figure 1. Structure of carbon nanotubes [12].

The dimensions of CNTs vary over a wide range. The diameters of SWCNTs are usually 0.4–3 nm, and their lengths range from a few tens of nanometers to several centimeters. To understand the structure and properties of CNTs, the bonding structure and properties of carbon atoms should first be described. A carbon atom has six electrons, with two of them filling the 1s orbital. The remaining four electrons fill the sp^3 or sp^2 as well as sp hybrid orbital, responsible for the bonding structures of diamond, graphite, nanotubes, or fullerenes. In diamond, the four valence electrons of each carbon occupy the sp^3 hybrid orbital. In graphite, three outer-shell electrons of each carbon atom occupy the planar sp^2 hybrid orbital. Bonding in CNTs is essentially sp^2. However, the circular curvature will cause quantum confinement and σ-π rehybridization in which three σ bonds are slightly out of plane; to compensate, the π orbital is more delocalized on the outside of the CNT. This makes CNTs mechanically stronger, and electrically and thermally more conductive than graphite [13].

Depending on the manner in which the graphene sheet is rolled up, the arrangement of carbon atoms along the cylinder circumference can be “arm-chair”, “zig-zag”, or several different intermediate chiral structures (Figure 2). The arrangement of the hexagons in the cylinder is referred to as the chirality and is defined in terms of indices (*n*,*m*). The chirality of the graphene sheet determines the electrical conductivity of the SWCNT. Metallic SWCNTs have equal *n* and *m*. When $n - m$ is a multiple of three, the SWCNT is semimetallic, while all other combinations result in semiconductor SWCNTs [14].

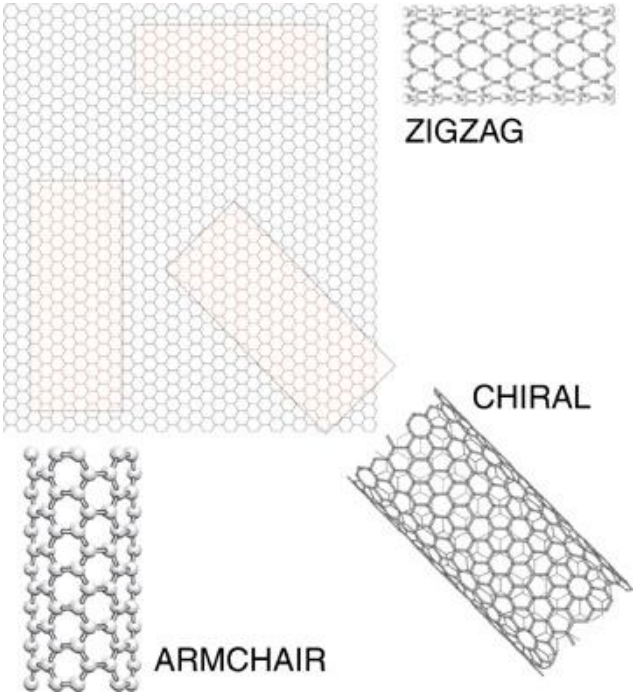

Figure 2. Chiral structure of carbon nanotubes [15].

CNTs and especially SWCNTs were found to have exceptional mechanical, thermal, and electronic properties [10,11,14]. A brief summary of the physical properties of SWCNTs and materials made of SWCNTs is presented in Table 1.

Many potential applications have been proposed for CNTs, such as their use in reinforcement composite materials [16–18], nano-transistors [19–21], AFM/STM tips [22–24], transparent and flexible electrodes [25,26], and electron-field emitters [27,28].

Thin SWCNT films can exhibit conductivity/transmittance values comparable to those of low-temperature ITO and, in particular, transparent conducting SWCNT coatings on flexible substrates such as polyethylene terephthalate (PET) outperform ITO/PET

electrodes in terms of chemical and mechanical stability and exhibit a wider electrochemical window [26,29].

Table 1. Physical properties of individual SWCNTs and materials made of SWCNTs.

Individual SWCNTs		Ref.
Young's modulus of elasticity	300–1470 GPa (compared to 200 GPa for high-strength steel)	[30]
Tensile strength	30–200 GPa (compared to 1–2 GPa for high-strength steel)	[30,31]
Thermal conductivity along the tube	~6600 W/(m·K) (twice as high as that of diamond)	[32]
Electrical resistance of metallic CNTs	3×10^{-6} Ω·cm at 300 K (compared to 2.82×10^{-6} Ω·cm for Al and 1.72×10^{-6} Ω·cm for Cu)	[33,34]
Maximum current density (without destruction)	10^9 A/cm^2, with a theoretical limit of 10^{13} A/cm^2 (compared to 10^7 A/cm^2 for copper wire of 100 nm in diameter)	[35–37]
Hole and electron mobilities	$(2–6)\times10^4$ cm^2/Vs (compared to 450 and 1400 cm^2/Vs for Si at 300 K)	[38]

In addition, the application of SWCNTs as field-emission electron sources for use in flat-panel displays, lamps, gas-discharge tubes, X-ray sources, and microwave generators has been widely explored. The advantages of these devices over those made from conventional metals such as tungsten and molybdenum are the following: relatively easy manufacturing/fabrication process, less deterioration in moderate vacuum (10^{-8} Torr), and high current densities of ~10^9 A/cm^2 [28].

Other desirable properties that make CNTs promising materials as field emitters are their nanosize diameter, structural integrity, high electrical conductivity, and high chemical stability. Notwithstanding these favourable advantages, CNT-based emission devices face stiff competition from liquid-crystal panel displays and other organic and polymeric light-emitting-diode displays [39].

Studies on a field-effect transistor made from a semiconducting SWCNT showed it to have the ability to be switched from a conducting to an insulating state. Logic switches,

the basic components of computers, can be constructed by coupling such CNT transistors [18,39].

Recently, the application of random CNT networks (CNTNs) as semiconducting materials for thin-film transistors (TFT) has attracted interest due to their superior performance compared to that of organic TFTs and potentially low-cost fabrication [19,20]. Uniformity of CNTN properties is achieved by statistical averaging over the large number of individual tubes that make up the network. Various devices and components based on CNTNs have been successfully demonstrated, including diodes, logic circuit elements, solar cells, displays, and sensors [19,20].

2.2 Synthesis of carbon nanotubes

All CNT synthesis methods can be classified according to the type of carbon atomization as either physical or chemical techniques. Physical production involves high energy input to the carbon source (graphite or carbon black) by arc-discharge or laser evaporation [40–42]. For the synthesis of SWCNTs, a small amount of metal catalyst is added.

Arc discharge. The carbon arc-discharge method was initially used for producing C_{60} fullerenes. However, this technique produces a mixture of SWCNTs, MWCNTs, fullerenes, and amorphous carbon, making purification a necessary process step, which involves separating the nanotubes from the soot and the catalytic metals present in the crude product. This method creates nanotubes through arc-discharge between two carbon rods placed end to end, separated by approximately 1 mm, in an enclosure that is usually filled with an inert gas (helium, argon) at low pressure (between 50 and 700 mbar) (Fig. 3).

Recent investigations have shown that it is also possible to create nanotubes by an arc method in liquid nitrogen [43]. A direct current of 50 to 100 A driven by approximately 20 V creates a high-temperature discharge between two electrodes. The discharge vaporizes one of the carbon rods and forms a small rod-shaped deposit on the other rod [4].

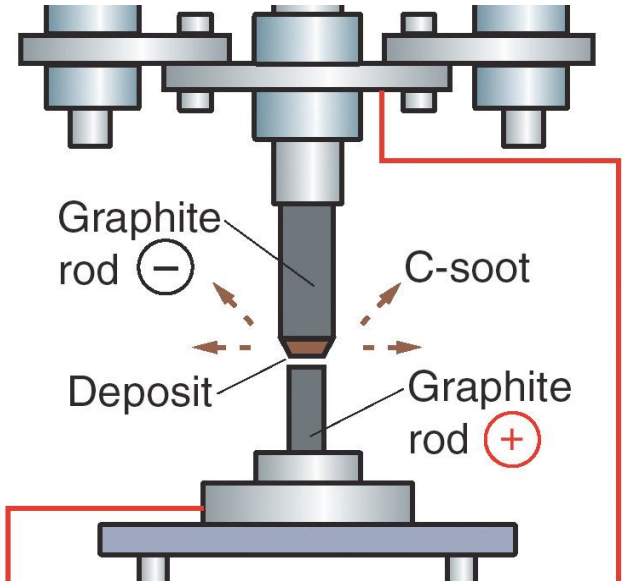

Figure 3. Schematic representation of the arc-discharge system [44].

Laser ablation. In 1995, Smalley's group [45] at Rice University reported the synthesis of CNTs by laser vaporization. A pulsed [46,47] or continuous [48,49] laser was used to vaporize a graphite target in an oven at 1200 °C. The main difference between the continuous and pulsed lasers is that the pulsed laser demands a much higher light intensity (100 kW/cm^2 compared with 12 kW/cm^2) (Figure 4). The oven is filled with helium or argon gas in order to keep the pressure at 500 Torr.

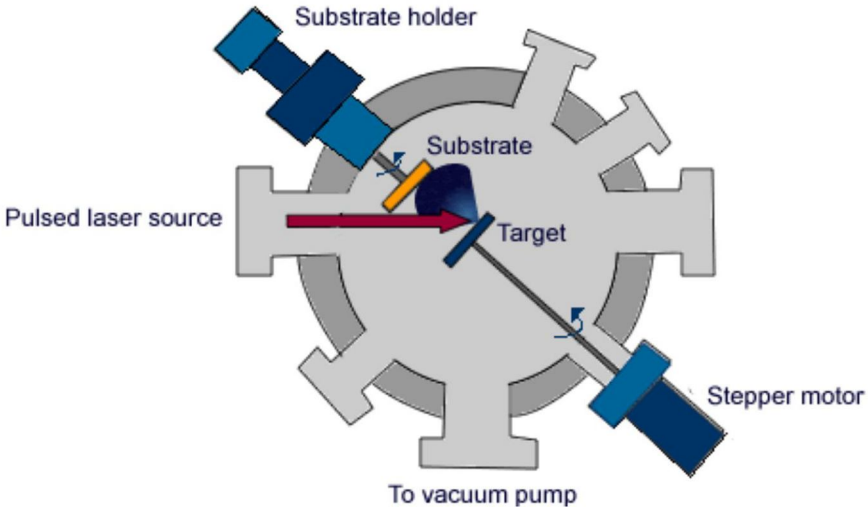

Figure 4. Schematic representation of the laser ablation system [50].

Chemical vapour deposition. The chemical route is based on the catalytic decomposition of carbon-containing precursors. The obvious advantage of this method is the possibility of producing CNTs at relatively low temperatures. The chemical methods can be divided into substrate CVD [e.g., 51–53] and free-floating catalyst (aerosol unsupported) CVD synthesis [e.g., 54–56]. In the substrate CVD process, decomposition of the carbon precursor and CNT formation take place on the surface of catalyst particles that are supported on a substrate, commonly aluminium oxide or silicon dioxide.

In the free-floating catalyst method, the whole process takes place in the gas phase or on the surface of catalyst particles suspended in a gas. As catalysts, transition metals such as Fe, Co, or Ni are commonly used. One of the first floating catalyst techniques, the HiPco process, was developed by Nikolaev *et al.* at Rice University in 1999 [57,58]. HiPco is based on CO disproportionation on the surface of iron particles. The catalyst is generated *in situ* by thermal decomposition of iron pentacarbonyl ($Fe(CO)_5$) in a reactor heated to 1000–1200 °C. The HiPco process is operated at high CO pressures (up to 50 bar), which significantly increases the CO disproportionation rate and thus enhances the SWCNT yield. SWCNT synthesis methods studied in this thesis, the ferrocene-based method and the hot-wire generator method, are also floating catalyst methods.

3 Experimental

3.1 Synthesis: HWG and ferrocene-based reactors

For the synthesis of SWCNTs and nanobuds, and for the investigation of their formation mechanisms, two different experimental set-ups were used. The first experimental set-up consisted of a hot-wire generator (HWG) of catalyst particles and a heated vertical tubular reactor (Figure 5) (Papers II, III, V). The alumina ceramic tube used for the experiments contained SiO_2 (0.25%), Ca (0.02%), Fe (0.02%), and Cd (0.09%) as impurities.

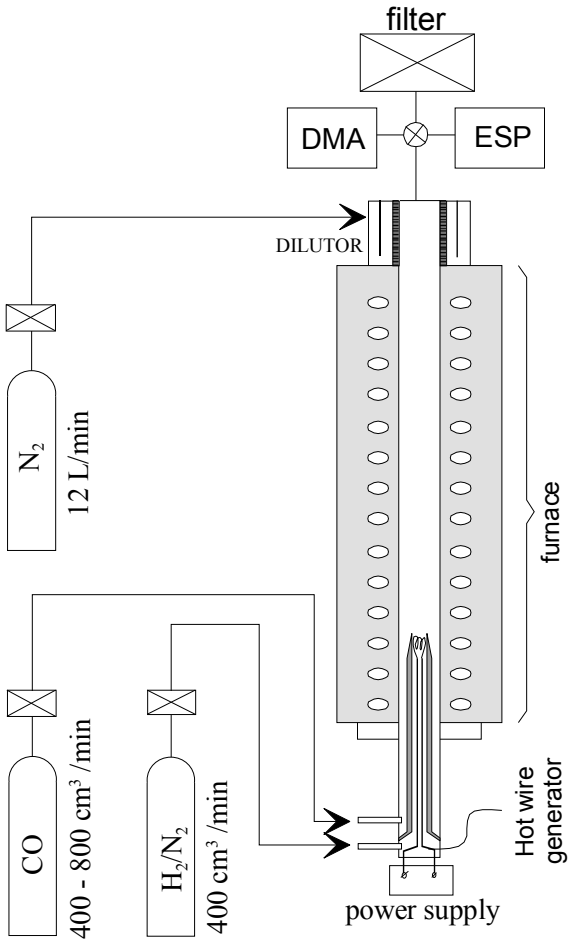

Figure 5. Schematic representation of the HWG method.

A tube with an internal diameter of 22 mm inserted inside a furnace of length 90 cm was used as the reactor. Another ceramic tube with external and internal diameters of 13 and 9 mm, respectively, and of length 25 cm was inserted into the reactor in order to protect the HWG from the CO atmosphere. Hereinafter, this method will be referred to as the HWG method.

The HWG consisted of a resistively heated thin iron wire (0.25 mm in diameter) located inside the internal tube. The location of the internal tube and the hot wire could be adjusted. The metal particles produced by the HWG were carried into the reactor with nitrogen/hydrogen (with a mole component ratio of 93.0/7.0). In the reactor, the flow containing the aerosol metal particles from the HWG was mixed with the outer CO flow (400 cm^3/min). Inside the reactor, CO disproportionation (Boudouard reaction)

$$CO_{(g)} + CO_{(g)} \leftrightarrow C_{(s)} + CO_{2(g)} \quad (1)$$

and hydrogenation

$$H_{2(g)} + CO_{(g)} \leftrightarrow C_{(s)} + H_2O_{(g)} \quad (2)$$

reactions took place on the surface of these metal particles. A porous tube dilutor (12 L/min flow of N_2) was installed downstream of the reactor to prevent SWCNT deposition on the walls.

The second experimental method (Figure 6) was based on ferrocene vapour decomposition (Papers I–IV, VI, VII). The experimental set-up included a precursor feed system, a furnace of length 55 cm equipped with a ceramic tube, as well as sampling and analysis devices. Carbon monoxide (CO) was used both as a carrier gas and as the carbon precursor. To vaporize ferrocene, a flow of CO (300 cm^3/min) was continuously directed through a cartridge containing the precursor powder mixed with SiO_2 powder at ambient temperature. A stainless steel water-cooled injector probe, held constantly at 24 °C, was used to feed the precursors to the furnace. The location of the injector probe was varied in order to control the precursor vapour heating rate and the residence time in the furnace. The temperature at which the precursor was introduced was determined by the furnace wall temperature and varied only slightly depending on the vertical location of the injector probe inside the furnace. An additional CO flow of

100 cm^3/min was introduced outside of the water-cooled probe. A constant partial pressure of 0.7 Pa of ferrocene vapour was introduced into the reactor.

Downstream of the furnace, the aerosol was diluted with 12 L/min of pure, ambient temperature N_2 to reduce losses on the reactor walls due to diffusion and thermophoresis and to decrease SWCNT agglomeration. Moreover, the dilutor was used to lower the gas temperature downstream of the reactor. Alternatively, the dilutor was removed and samples were collected by filtration through silver or nitrocellulose filters at the outlet of the furnace at ambient temperature.

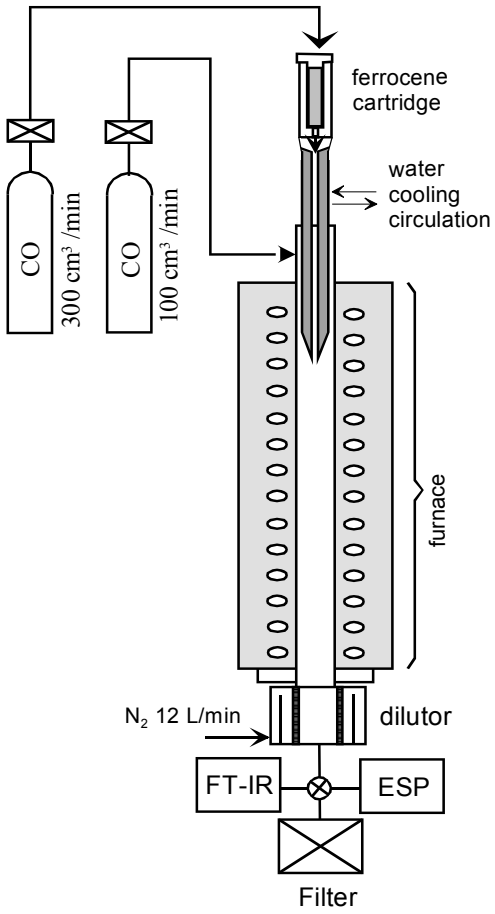

Figure 6. Schematic representation of the ferrocene reactor.

For the synthesis of nanobuds in both reactors, controlled amounts of H_2O vapour and CO_2 were introduced together with the CO. A mass flow controller was used for additional introduction of CO_2 and/or H_2O vapour. In order to introduce the H_2O vapour, a flow of a carrier gas was passed through a water saturation vessel. The

amount of introduced H_2O vapour was varied from 0 to 405 ppm. The concentration of introduced CO_2 was varied from 0 to 5000 ppm in the HWG case and from 0 to 12000 ppm in the ferrocene case.

3.2 Characterization methods and techniques

Following fabrication by both methods, the samples were collected downstream of the reactor either on 2.45 cm diameter nitrocellulose (or silver) disk filters (Millipore Corp., USA) (Papers I–III, VI, VII) or on transmission electron microscopy (TEM) grids by an electrostatic precipitator (ESP) (Papers I–VII). The morphology and crystallinity of the products were investigated with a field emission gun transmission electron microscope (Philips CM200 FEG) (Papers I–VII) operating at an accelerating voltage of 200 kV or with a transmission electron microscope equipped with an imaging Cs-corrector (FEI Titan 80-300) operating at an accelerating voltage of 300 kV (Paper I). Chemical elemental analysis of the as-produced samples of nanobuds by means of electron energy loss spectroscopy was performed with a field emission transmission electron microscope (Philips CM200 FEG) (Paper III).

The aerosol number size distributions of the gas-phase samples were measured continuously at the outlet of the reactor with a DMA system [59,60]. The DMA system consisted of a classifier (TSI 3081) with a sample flow rate of 0.3 L/min and a sheath flow rate of 6 L/min of N_2, a condensation particle counter (TSI 3022), and a ^{241}Am bipolar charger (optional). The classifier contained two electrodes, between which charged aerosol particles were classified according to their electrical mobility, which, in turn, was dependent on both the size and electrical charge of the particles. This method allows unambiguous delineation of the conditions of SWCNT formation, without having to resort to time-consuming transmission electron microscopy (TEM) observations. Adequate power supplies for applying both positive and negative polarity to the classifier internal electrode were used, while the external electrode was kept grounded.

In order to study the charging state of the naturally charged SWCNTs, tandem DMA measurements were carried out. For this purpose, a Hauke DMA classifier with a sample flow rate of 1.5 L/min and a sheath flow rate of 15 L/min (N_2) was used to extract fractions of certain mobility-sized SWCNTs, which were then introduced into a second TSI DMA via a ^{85}Kr charger (Figure 7).

An electrostatic filter (ESF) located downstream of the reactor was used to filter out all charged aerosol products from the gas phase by applying an electric field. It comprised two metallic plates with dimensions of 15 cm in length and 1.5 cm in width separated from each other by a distance of 1 cm. An electric field was created by connecting one of the plates to a high voltage (4 kV) source, while the other one was kept grounded.

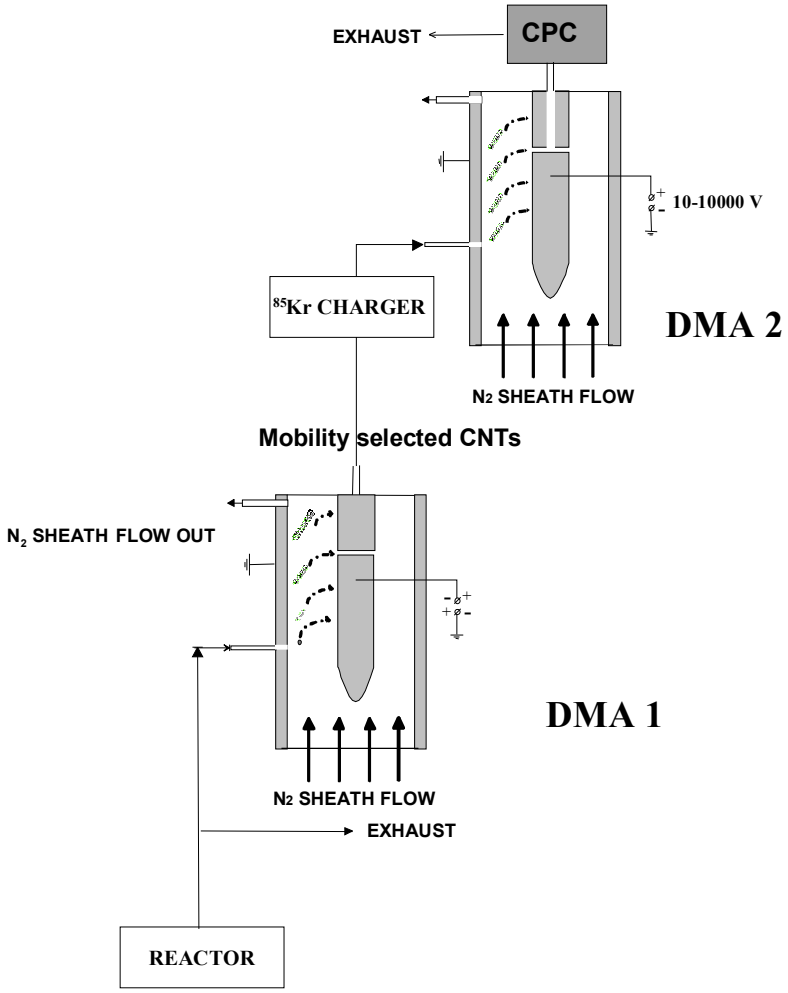

Figure 7. Schematic representation of the tandem DMA system.

In order to sample the SWCNTs *in situ*, a stainless steel sampling rod with a TEM grid attached to the top was rapidly inserted into the reactor and held in a steady position for 30 s. The sample was collected due to the thermophoretic forces between the hot atmosphere in the reactor and the cold sampling rod (Papers I, IV).

Fourier-transform infrared spectroscopy (FT-IR) was applied to study the disproportionation reactions of ferrocene and CO during the SWCNT synthesis (Papers III, VI). The FTIR measurements were mainly used to study the conversion of CO to CO_2. The FTIR instrument (GASMET DX4000, Temes Instruments) was fitted with a 1 dm^3 flow-through cuvette and the measurement temperature was 45 ºC.

In order to examine the nature of the ions emitted from the SWCNTs, which could be responsible for SWCNT ionization, laser desorption ionization time-of-flight spectrometry (LDI-TOF) measurements were carried out with a Voyager-D STR MALDI-TOF mass spectrometer. For this purpose, SWCNT samples were collected on a silver filter as a powder and transferred to an LDI-TOF steel sample substrate (Paper VI).

The layer thickness of the collected SWCNT mats was measured with a scanning electron microscope (SEM, LEO DSM-982 GEMINI) and an atomic force microscope (AFM). Eight cross-sections of SWCNT mat samples at different mat positions (three in the centre and five at the edges) were measured and averaged (Paper VII).

Electron FE measurements on randomly oriented mats of SWCNTs and nanobuds were performed using a 2 mm hole and 450 μm and 675 μm spacers between the cathode and anode. Cold electron field emission measurements were carried out at a chamber pressure below 5×10^{-7} Torr. A 5 kV Keithley 248 power supply and a Keithley 6517A electrometer with pA precision were used for electric field generation and emission current monitoring, respectively (Paper III).

The Raman spectra of the nanobud samples were measured under excitation with 633, 514, and 488 nm lasers (Paper III).

4 Results and Discussion

4.1 Control and optimization of aerosol synthesis

Initially, the synthesis of SWCNTs in the HWG and ferrocene reactors was unstable. Analysis of the experimental data showed that these instabilities were primarily associated with the reactor wall conditions. It was found that for stable SWCNT synthesis the wall of the reactor had to contain a catalyst material. This could be realized by deposition of a catalyst on the reactor walls or by using a reactor tube made out of the catalyst material, e.g. stainless steel.

Further investigations showed that for stable SWCNT synthesis the introduction of a small concentration of an etching reagent such as CO_2 or H_2O was needed. FT-IR measurements showed that the main gaseous product of CO disproportionation was CO_2, with concentrations of 120 and 1540 ppm in the HWG method and the ferrocene set-up, respectively.

In order to clarify the roles of CO_2 and H_2O during SWCNT synthesis, experiments were carried out in a "clean" wall reactor. An HWG reactor, made from a ceramic tube, was mechanically cleaned and baked at 1200 °C, thereby removing all catalyst material from the walls. It was found that no SWCNTs were produced when pure CO was used. Introducing 1000 ppm CO_2 into the clean HWG reactor resulted in SWCNT formation. Figures 8a,b show respective TEM images of the typical products synthesized in the presence of "native" CO_2 and when 1000 ppm CO_2 was introduced into the "clean" reactor. A clear effect on the morphology of the produced SWCNTs can be observed. The TEM images show that the lengths of the SWCNT bundles increased from approximately 300 nm to more than 1 μm when additional CO_2 was introduced into the reactor. Also, the lengths of the individual SWCNTs increased from 60 nm up to 300 nm. The optimal CO_2 concentration for SWCNT growth was found to be between 80 and 1500 ppm in the case of the HWG reactor. At a CO_2 concentration of 1750 ppm, a

portion of the catalyst particles becomes inactive for the initiation of the CNT formation.

H_2O vapour is also always present among the effluent gases from reactors having iron on their walls due to the catalytic CO hydrogenation reaction on these walls. Experiments were carried out in both reactors in which 150 or 330 ppm of H_2O vapour was introduced in addition to the "native" H_2O formed on the reactor walls. The TEM image in Figure 8c shows an increase in the SWCNT bundle length compared to those fabricated under conditions when neither CO_2 nor H_2O was additionally introduced (Figure 8a).

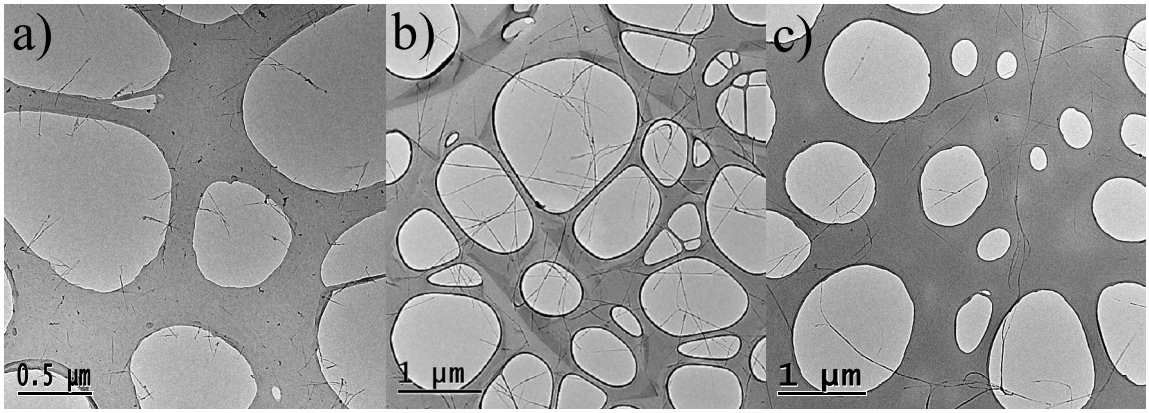

Figure 8. TEM images of SWCNTs synthesized in HWG reactor under conditions: a) when CO_2 and H_2O were formed on the reactor walls (CO_2 – about 100 ppm, H_2O – about 10 ppm); b) when 1000 ppm CO_2 was introduced; c) when 150 pp H_2O was introduced.

The experimental results showed that in the HWG reactor the presence of CO_2 and H_2O in the system can significantly alter the growth of the SWCNTs. The possible function of CO_2 and H_2O may be to etch amorphous carbon that might otherwise poison the catalyst particles needed for SWCNT nucleation and growth. The catalyst particles play two important roles: they catalyze the CO disproportionation reaction that produces free carbon for SWCNT production and they determine the diameter of the produced SWCNTs. Additionally, steady-state growth of SWCNTs cannot proceed if the surface of the catalyst particle is poisoned by amorphous carbon. Importantly, the reaction of CO_2 (or H_2O) with amorphous carbon is more energetically favourable than that with carbon integrated in the graphene layer.

4.2 Carbon nanobuds

Variation of the H_2O vapour or CO_2 concentrations introduced into the reactor allowed us to synthesize SWCNTs covered with covalently attached fullerenes. This material was termed carbon nanobuds, since the fullerenes on the surface of the SWCNTs were reminiscent of buds on a branch (Figure 9).

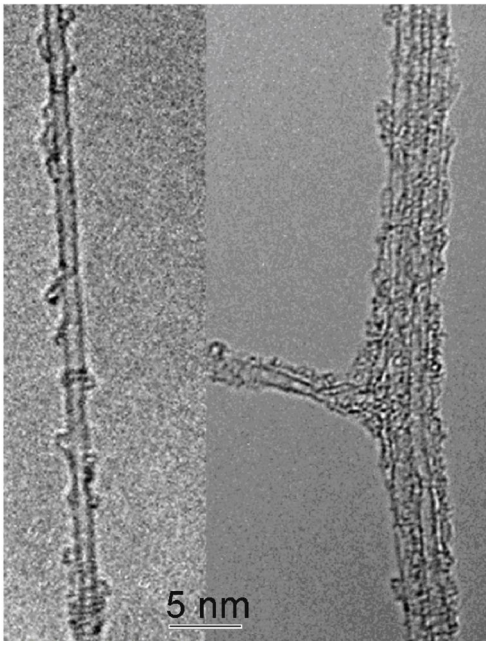

Figure 9. TEM images of a carbon nanobud sample, revealing the presence of spherical structures on the surface of the SWCNTs.

In an attempt to control the density of fullerenes on the SWCNTs, systematic investigations on the effect of the reactor temperature and of the concentrations of H_2O vapour and CO_2 were carried out. These parameters were found to have a noticeable effect on the density of fullerenes on the surface of the tubes. The introduction of H_2O or CO_2 into the ferrocene reactor revealed that the optimal concentrations were between 45 and 245 ppm for H_2O and between 2000 and 6000 ppm for CO_2, with the highest fullerene density on individual SWCNTs being in excess of 1 fullerene/nm. The preferred conditions for nanobud formation were identified as an H_2O concentration between 125 and 185 ppm and a CO_2 concentration of approximately 2500 ppm.

An example of the change of the nanobud morphology with the reactor conditions is shown in Figure 10, wherein the effect of H_2O vapour concentration in the reactor at a

temperature of 1000 °C can clearly be seen. Experimental conditions without the addition of H_2O resulted in the formation of largely pure SWCNTs together with non-active catalyst particles. Nanobuds started to form in abundance at H_2O vapour concentrations of 45 ppm and above. Conversely, at high concentrations of H_2O (>365 ppm), the sample contained a high fraction of inactive catalyst particles and few nanobuds.

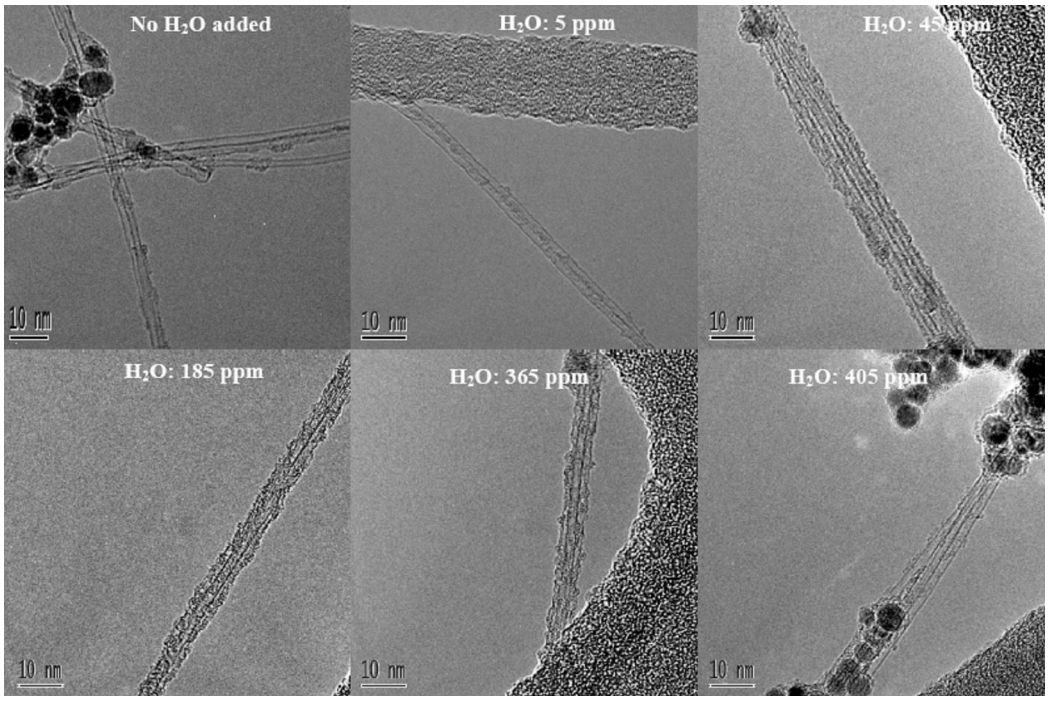

Figure 10. Effect of the concentration of the water vapour introduced into the ferrocene reactor at 1000 °C.

In addition to TEM observations, the presence of fullerenes on the SWCNT surface was proved by means of STM, MALDI-TOF MS, and UV/vis absorption measurements. Their covalent attachment to the outer walls of the SWCNTs was examined by their dissolution and evaporation from the SWCNT surface.

In order to understand the nature of the bonding between fullerenes and SWCNTs, atomistic density functional theory (DFT)-based calculations were carried out. The calculations showed that systems composed of fullerenes covalently bonded through ester groups to single-vacancy SWCNTs can indeed exist (Figure 11a). Calculations with a model Hamiltonian showed that fullerenes can be directly covalently bonded to SWCNTs or can form hybrid structures.

Results for the different adsorption scenarios of fullerenes on an (8,8) SWCNT are summarized in Figures 11b and 11c. It was found that the structure formed by the chemisorption of perfect C_{60} molecules on SWCNTs (Figure 11b) is quite stable, but that the configuration becomes unstable or only marginally stable with respect to a defective SWCNT and an isolated fullerene (Figure 11c). One of the viable hybrid geometries involves imperfect fullerenes covalently bonded to defective SWCNTs. Such bonded structures, with a neck connecting the fullerene and the SWCNT, are depicted in Figures 11d and 11e. The local binding energies in these structures (represented in colour) suggest that none of the carbon atoms are less stable than those in a C_{60} molecule.

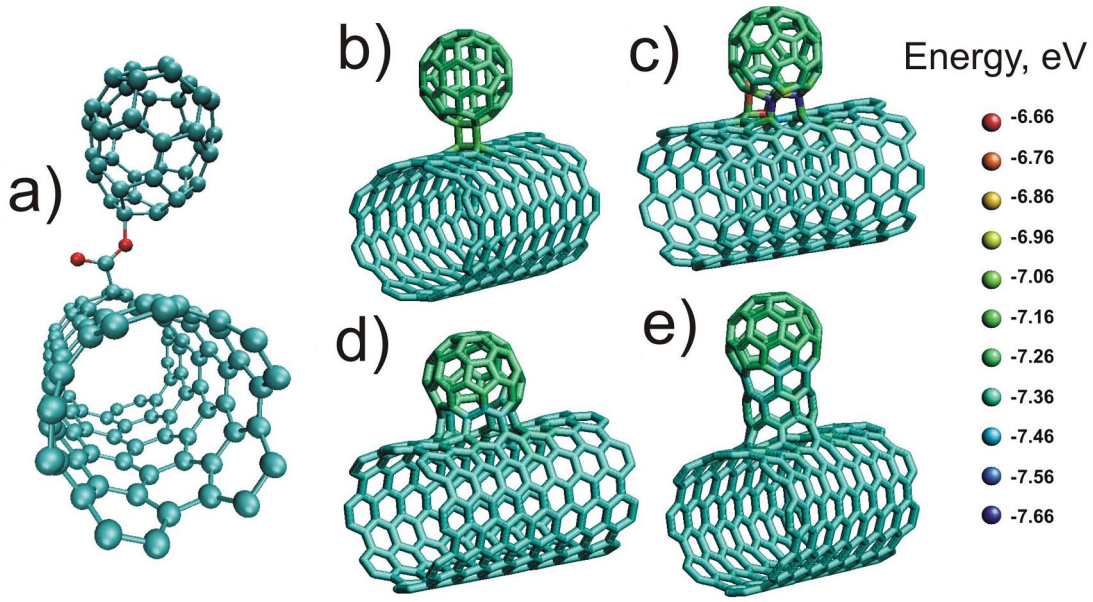

Figure 11. Bonding scenarios of fullerenes on SWNTs: (a) C_{42} connected with a SWNT via an ester group; (b,c) C_{60} chemisorbed on a defect-free (8,8) SWNT; (d, e) fullerene-SWNT hybrid structures, reminiscent of buds on a branch. (Courtesy of Dr. A.V. Krasheninnikov).

In situ experiments were performed to study nanobud formation. It might have been assumed that fullerenes were formed in the reactor separately from SWCNTs and then deposited on their surface at the outlet of the reactor. However, it was shown by *in situ* sampling experiments that fullerenes were present in all samples in which SWCNTs were detected. Thus, one can conclude that SWCNTs and fullerenes were formed simultaneously. TEM observations suggest that both fullerenes and SWCNTs originate from graphitic carbon precipitated on the surface of Fe nanoparticles catalyzing CO

disproportionation [5,61,62]. This is supported by the results of molecular dynamics simulations, which indicate that various curved carbon nanostructures (fullerenes or fullerene-like structures) can be formed on the surface of catalyst particles [63,64]. It was proposed that the growth of SWCNTs occurs in a steady-state regime by the provision of additional carbon from reactions (1) and (2) at the catalyst surface to the edge of the carbon layer. Therefore, the formation of SWCNTs occurs in the temperature range between 885 and 945 ºC, in which the inverse reactions (1) and (2) are significant either due to the introduction or formation of H_2O vapour and CO_2 upstream of the reactor.

Before discussion of the nanobud formation mechanism, the observed nanobud structures should be classified. The first type, fullerenes on the surface of SWCNTs, can possess a complete spherical structure and can be covalently bonded to SWCNTs through sp^3-hybridized carbon atoms (Figures 11a–c). The second type, in which all carbon atoms are sp^2-hybridized, can be described as a fully hybrid structure, where a fullerene forms a continuous part of a SWCNT (Figure 11d,e). Nevertheless, irrespective of the structure of the nanobuds, initially a certain number of pentagons should be generated for fullerene formation. It is known that for fullerene formation, 12 pentagons are needed. The formation route of these pentagons, promoted by the presence of etching molecules, is expected to determine the formation of fullerenes. Figure 12 schematically depicts our understanding of the formation of pentagons on the surface of a catalyst particle.

Carbon atoms at the edge of the dynamic layer (with dangling bonds) can be attacked by etching molecules such as H_2O. This results in the release of CO and H_2 and in the closure of rings consisting of five carbon atoms (pentagon formation). Further, the former pentagon can be surrounded by hexagons, and new pentagons can be formed as indicated in the suggested schematics. According to the proposed mechanism, the concentration of etching molecules should have some optimal value, since a low concentration of oxidants will lead to the formation of pure SWCNTs (without fullerenes), while high concentrations should suppress the formation of SWCNTs because of excess positive curvature.

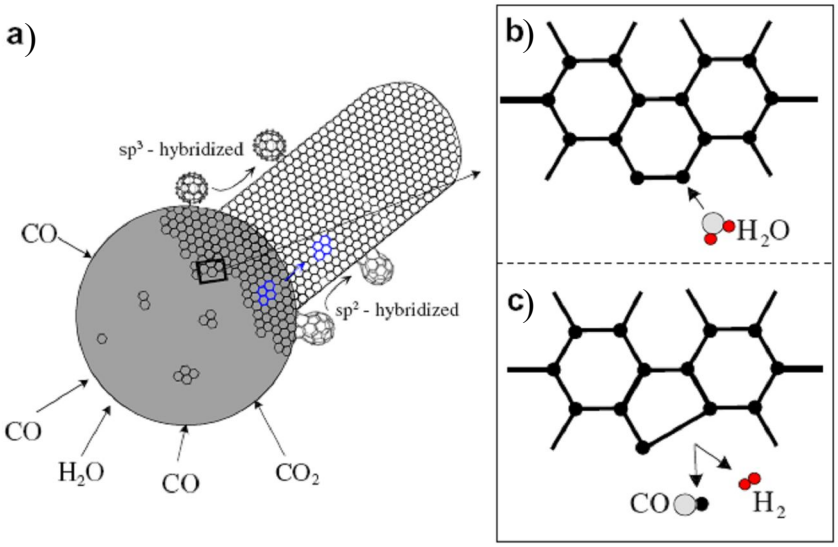

Figure 12. Schematic representations of (a) nanobud growth by continuous transportation of a carbon layer from a particle to a SWCNT, (b) pentagon formation at the edge of the dynamic layer of a growing SWCNT, and (c) the growth mechanism of nanobuds.

4.3 Charging phenomena

4.3.1 Separation of individual carbon nanotubes

The DMA is a standard tool in the field of aerosol science for determining particle number size distributions in the gas phase. The DMA system consists of a classifier, a condensation particle counter, and a ^{241}Am bipolar charger (optional). However, DMA measurements obtained without the charger prior to the DMA revealed that the SWCNTs coming from the HWG reactor were naturally charged and did not need to be charged to be measured by the DMA system. Moreover, it was found that the higher the concentration of SWCNTs, the higher the charging. This fact is believed to be related to bundling of the SWCNTs, since the probability of bundling increases with their concentration in the gas phase. Accordingly, the natural charging of the SWCNTs may occur due to the formation of bundles.

TEM observation of the sample collected downstream of the HWG reactor revealed the presence of both bundles and individual SWCNTs (Figure 13a). However, sample collection downstream of an operating ESF showed only the presence of individual SWCNTs (Figure 13b). This indicates that bundled SWCNTs were charged and trapped in the ESF, whereas individual SWCNTs were electrically neutral. To statistically confirm these results, careful TEM investigations were carried out. It was found that neutral SWCNTs consisted of 94% individual SWCNTs, and that a sample with 99% naturally charged SWCNTs contained 93% bundled SWCNTs. In both cases, the statistical sample involved 70 counts. The presence of a small fraction of charged individual SWCNTs can be explained in terms of thermal ion emission or collisions of neutral tubes with ions available in the gas phase. Conversely, the presence of a small fraction of neutral bundled SWCNTs may be related to possible SWCNT bundle discharge processes.

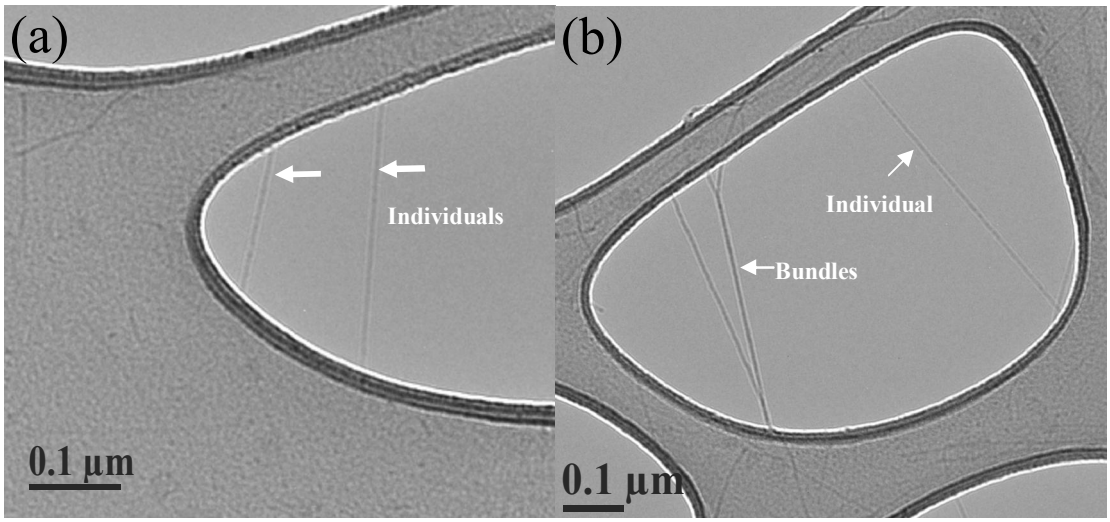

Figure 13. TEM images of (a) individual CNTs collected after filtering charged bundles with an ESF and (b) both individual and bundles of SWCNTs collected without ESF filtering.

On the basis of the fact that most of the individual SWCNTs were found to be electrically neutral, placing the electrostatic filter after the reactor allows the separation of individual and bundled SWCNTs. Since the sample collection is carried out at ambient temperature, this approach enables the deposition of individual SWCNTs on a wide variety of substrates, including those substrate materials that cannot withstand elevated temperatures.

4.3.2 Charging mechanism

Investigations of SWCNT formation by ferrocene vapour decomposition were carried out at 800, 1000, and 1150 °C in a CO atmosphere. The fraction of charged CNTs was determined on the basis of DMA size mobility measurements using a ^{85}Kr charger. Aerosol mobility size measurements were presented in two different ways: as distributions and as spectra. The mobility size distributions were measured by passing the aerosol-containing flow through a radioactive charger and then a typical inversion procedure was performed to calculate the real aerosol concentration assuming equilibrium charging in the charger [65]. The spectra, in which the concentration of the naturally charged aerosol was not subjected to the inversion procedure, were obtained without the charger. The mobility diameter, *D*, was calculated assuming spherically shaped and singly charged aerosol particles on the basis of the Millikan equation [66]. The concentrations of charged SWCNTs were very high (92% at 800 °C; 99% at 1000 °C; 98% at 1150 °C). Number size distributions of all and the noncharged fraction of SWCNTs synthesized at 1000 °C are presented in Figure 14.

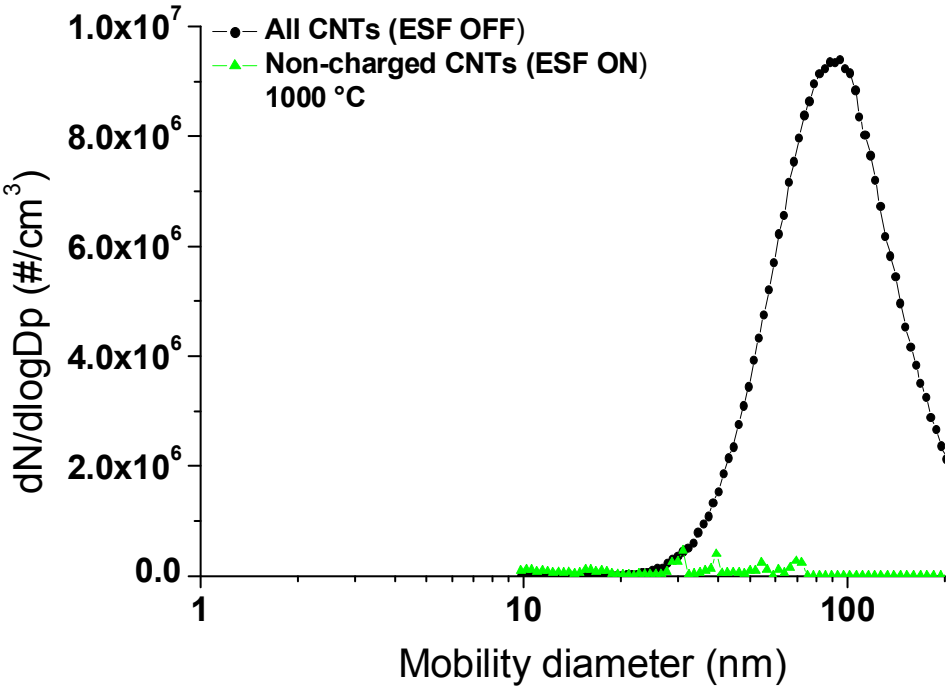

Figure 14. Number size distributions of all and the noncharged fraction of CNTs at 1000 °C.

At 800 °C, the concentration of negatively charged ions was found to be about 6 times higher than that of positively charged SWCNTs. Increasing the reactor temperature to 1000 °C resulted in an increase in the fraction of positively charged SWCNTs: the ratio between negatively and positively charged ion concentrations decreased to a factor of 2 (Figure 15). At 1150 °C, the spectra of both the negative and positive polarities were very similar.

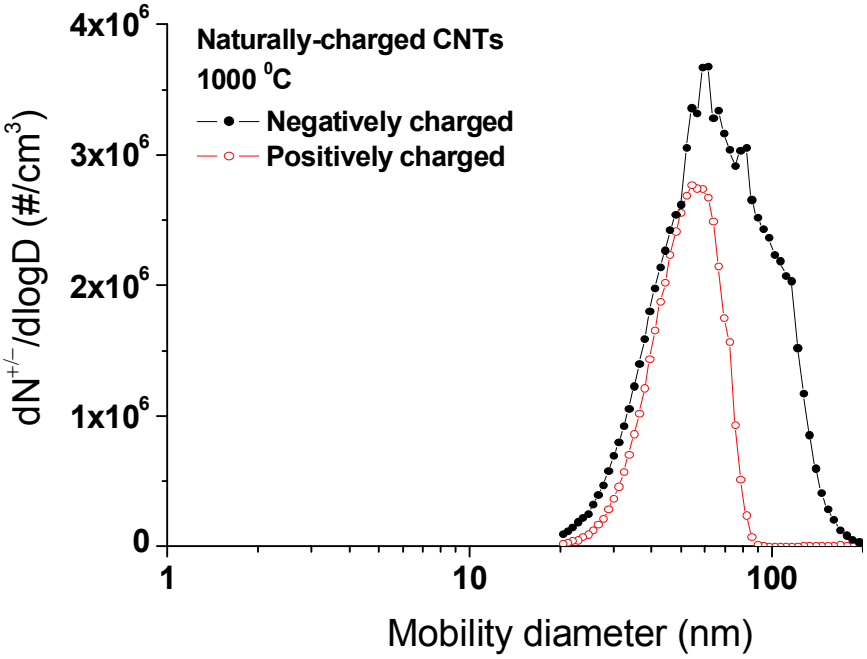

Figure 15. Mobility spectra of negatively and positively naturally charged CNTs at 1000 °C.

In order to study the charge state of the naturally charged SWCNTs, tandem DMA measurements were carried out (Figure 7). For this purpose, the first DMA was used to extract fractions of 80, 100, or 130 nm mobility-selected SWCNTs, which were then introduced into the second TSI DMA via a ^{85}Kr charger. The results of Gaussian function fittings with the measured standard geometric deviation showed that the SWCNTs possessed between 1 and 5 elementary charges (Figure 16).

In order to examine the nature of the ions that could be emitted from the SWCNTs, and hence could be responsible for the SWCNT ionization, LDI-TOF measurements were performed on the SWCNT samples, assuming that laser irradiation simulates the conditions inside the reactor. During the measurements, the power of the laser was varied from 0 to 3500 arbitrary units.

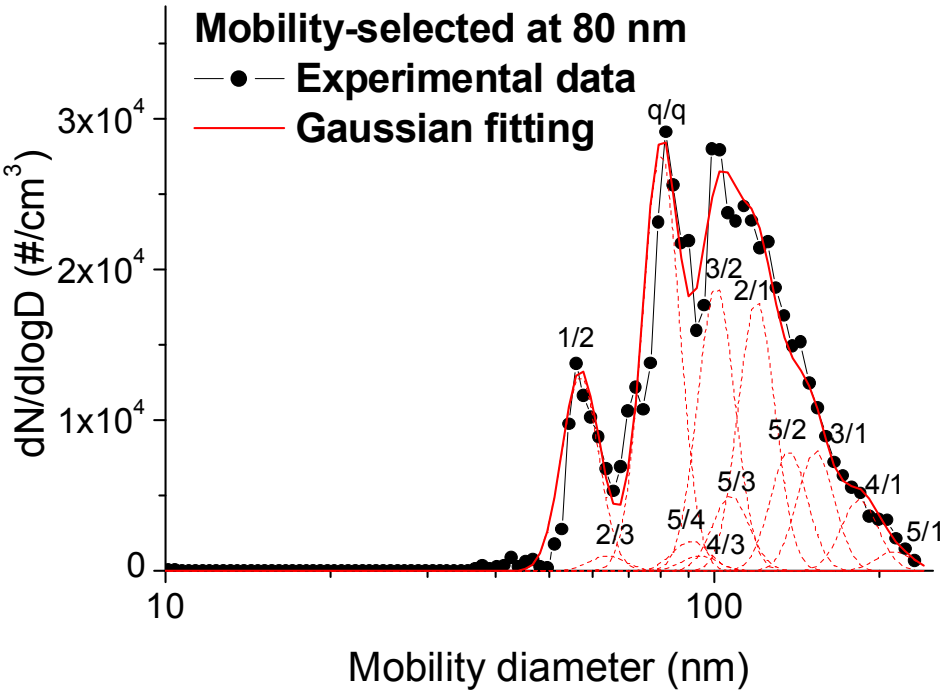

Figure 16. Results of tandem mobility measurements of naturally charged mobility-selected CNTs at 80 nm. Charge states are represented as follows: original number of charges/number of charges after passing through the neutralizer.

It was found that positively charged ions started to be detected at a power of about 2900 units (Figure 17a). Three strong peaks appeared at m/z = 91.07, 119, and 149 amu, which could be attributed to $C_6OH_3^+$, $C_7O_2H_3^+$, and $C_9O_2H_9^+$, respectively. Negatively charged ions appeared only at a high power of around 3200 power units, when the process of SWCNT destruction was already observed (Figure 17b).

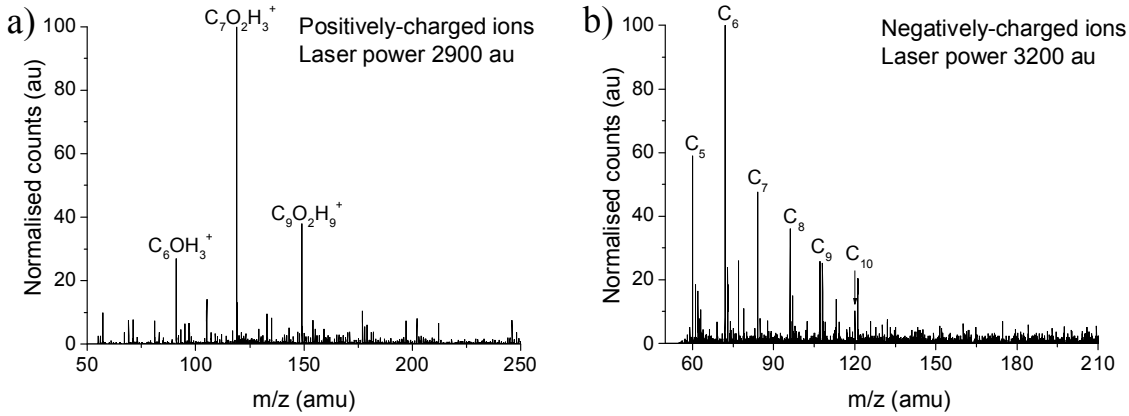

Figure 17. LDI-TOF spectra of ions released from CNTs at laser powers of (a) 2900 arbitrary power units (positively charged ions) and (b) 3500 power units (negatively charged ions).

At a laser power ≥ 3200 units, one could observe the formation of carbon clusters, C_5 (m/z = 60 amu), C_6 (72), C_7 (84), C_8 (96), C_9 (108), and C_{10} (120), in both the negative and positive modes. The ionization of positive ions therefore occurs at a much lower laser power, while no negative ions were detected before the onset of SWCNT destruction.

In order to explain the charging phenomenon, the presence of impurities with low adsorption energy has to be accepted. Positively charged ions can be emitted from the surface of SWCNTs at relatively low laser power. Chemically, these ions can be represented as long-chain carbon structures, akin to intermediates in the SWCNT growth process [67]. It is most likely that emission of ions of this kind was responsible for the negative charging of the SWCNTs. Since the LDI-TOF measurements could not detect negative ions emitted from the surface of the SWCNTs under laser irradiation, the SWCNT positive charging during bundling most likely occurred because of electron emission.

4.4 Carbon nanotube and nanobud formation mechanism

In order to investigate the SWCNT growth mechanism and kinetics, *in situ* experiments were performed using two different temperature profiles in the ferrocene reactor (Figure 18). The low temperature profile had a maximum temperature of 862 °C, while the high temperature profile had a maximum temperature of 1054 °C. In the case of the low temperature profile, the sample collected from a sampling point corresponding to a temperature of 816 °C did not reveal the presence of SWCNTs. Only inactive catalyst particles were seen by TEM observation. This position corresponds to the pre-nucleation SWCNT condition. SWCNTs were detected in samples collected downstream at sampling points corresponding to the following temperatures: 857 °C, 853 °C, 845 °C, and 763 °C.

Multiple measurements made from TEM images allowed determination of the average lengths of the SWCNTs collected at these different locations. The average length of individual SWCNTs collected at a temperature of 857 °C was 388 nm. At 845 °C and

763 °C, the average SWCNT lengths were 1225 and 1622 nm, respectively. Similar experiments were performed in the case of the high temperature profile. Surprisingly, the average lengths of SWCNTs collected at different locations over the high temperature profile were 290 nm throughout and did not depend on the position.

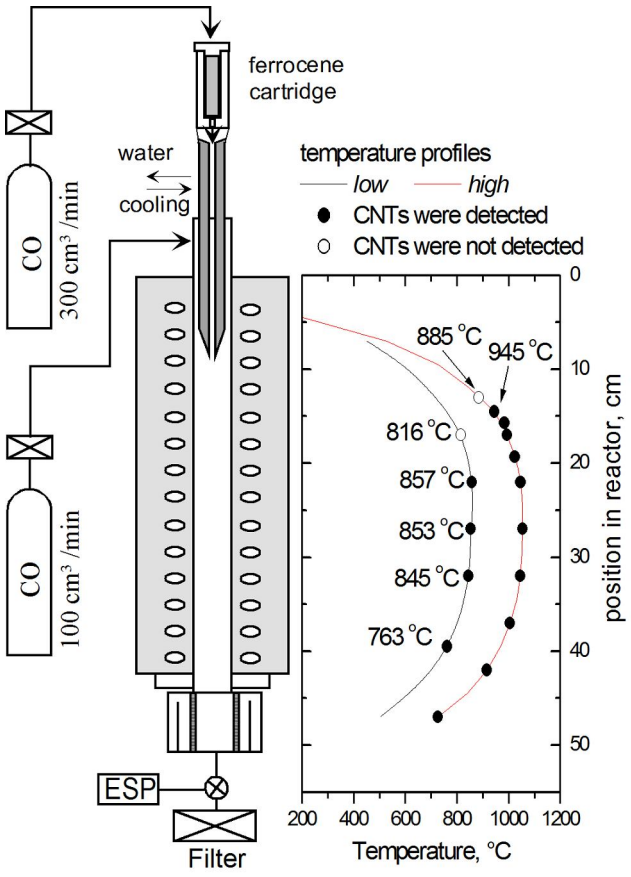

Figure 18. Schematic representation of the experimental set-up, temperature profiles, and positions inside the reactor used for in situ sampling of the product.

On the basis of the SWCNT length, temperature, and residence time in the reactor, the average growth rate of the SWCNTs could be calculated. The residence time was calculated as the distance between two sampling points divided by the average velocity of the gas flow. The calculations showed that, in the case of the low temperature profile, over the temperature ranges 816–857, 857–845, and 845–763 °C the average growth rates were 1.01, 1.11, and 0.67 μm/s, respectively. In the case of the high temperature profile, the average growth rate of the tubes with the length of 290 nm in the temperature range from 885 to 945 °C was calculated to be 2.7 μm/s.

Formally, the kinetics of SWCNT growth can be described by a process considering the transformation of carbon deposited on the surface of a catalyst particle into the hexagonal SWCNT carbon network:

$$C_{(s)} \rightarrow C_{SWCNT} \quad (3)$$

The rate of this reaction, r, can then be expressed in terms of the carbon concentration [C] on the surface of the catalyst particle:

$$r = k[C]^n = k_0[C]^n \exp\left(-\frac{E_a}{RT}\right) \quad (4)$$

where k and k_0 are the rate constant and the pre-exponential coefficient, respectively; n is the reaction order; E_a is the activation energy of the SWCNT growth; R is the gas constant; and T is the absolute temperature.

It is worth noting that the concentration of carbon on the surface of the catalyst particles does not determine the growth rate of SWCNTs. Otherwise, the highest growth rate would be observed at around 600–700 °C, the range in which the Boudouard reaction [61] has its maximum. Controversially, the conditions conducive to the maximum growth rate were those under which the disproportionation reaction rate was significantly suppressed thermodynamically. Therefore, the growth rate can be formally described in terms of a zeroth-order reaction (n = 0). Plotting the kinetic data of the growth rate in terms of the Arrhenius coordinates ln r *vs* 1/T gave a linear dependence (Figure 19), from which the pre-exponential coefficient and the activation energy were found to be $k_0 = 1.99 \times 10^6$ μm/s and E_a = 133.8 kJ/mol = 1.39 eV, respectively. In the figure, the temperature points correspond to the average temperature for each of the temperature ranges. This energy can be assigned as the activation energy for diffusion of carbon atoms in bulk solid iron with carbon concentrations ranging from 0.1 to 1 mass %. Thus, on the basis of the kinetic measurements, it can be concluded that the rate-limiting step for the growth of the SWCNTs is carbon diffusion through the solid catalyst particles.

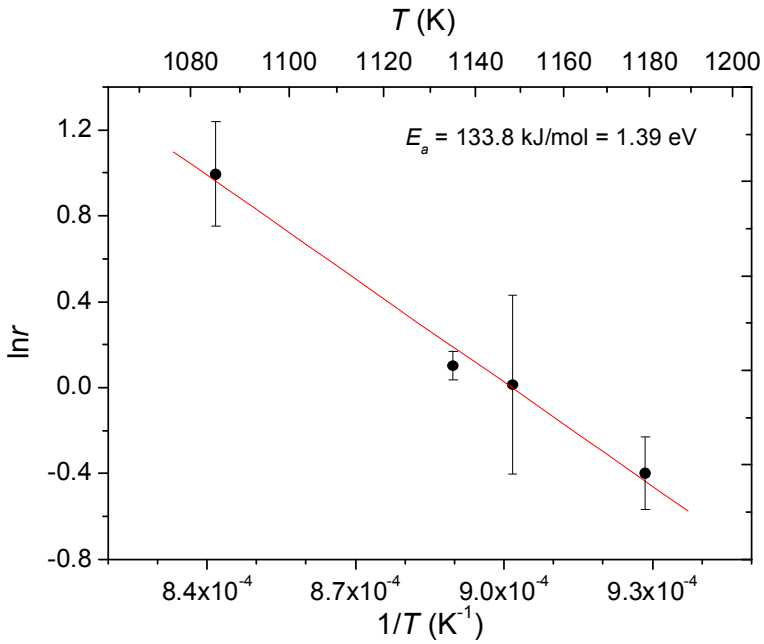

Figure 19. Kinetic dependence of ln *r* on inverse temperature revealing its linear behavior.

4.5 Demonstration of SWCNT and nanobud applications

Experiments on a single-step process for incorporating SWCNT mats of adjustable thickness, transparency, and conductivity into polymer substrates were carried out by a simple thermo-compression method. SWCNTs were first produced in a ferrocene reactor, and then SWCNT mats were collected directly from the gas phase downstream of the reactor by filtering through nitrocellulose (or silver) disk filters. Depending on the desired mat thickness, the deposition time was varied from a few minutes to several hours.

For the integration of SWCNT mats into PE films, the following procedure was performed. The PE film was placed on a heating plate and heated to 100 °C at a rate of 5–6 °C/min. PE films treated at this temperature were found to be the most transparent. Then, the aforementioned filter disk, coated with a SWCNT mat, was pressed against the heated PE film with a pressure of 0.35 N/cm^2 for 5–10 s. After removing the filter disk from the PE film, it was found that the SWCNT mat had been successfully

transferred. Double-sided lamination of SWCNT mats between PE films was also performed, as well as laminating several layers of PE films with SWCNT mats in series.

Since the as-deposited SWCNT mats had low density and, as a result, low contact between the tubes, prior to the measurements of the electrical properties, these mats were compacted by adding a droplet of ethanol to the transferred layer. For the electrical conductivity measurements, SWCNT mat samples of width 1 mm were placed on top of two copper electrodes with a gap between them of 1 mm. Addition of an ethanol droplet to the sample initially resulted in a sudden increase in the resistance, which was followed by an approximately constant rate of decrease during the ethanol evaporation process. After approximately 3 min, the resistance decreased to between 1.8 and 7.2 times lower than the original value. This significant decrease in resistance may be explained in terms of SWCNT film densification, increased inter-tube contact and, consequently, an improvement in the percolation between SWCNTs.

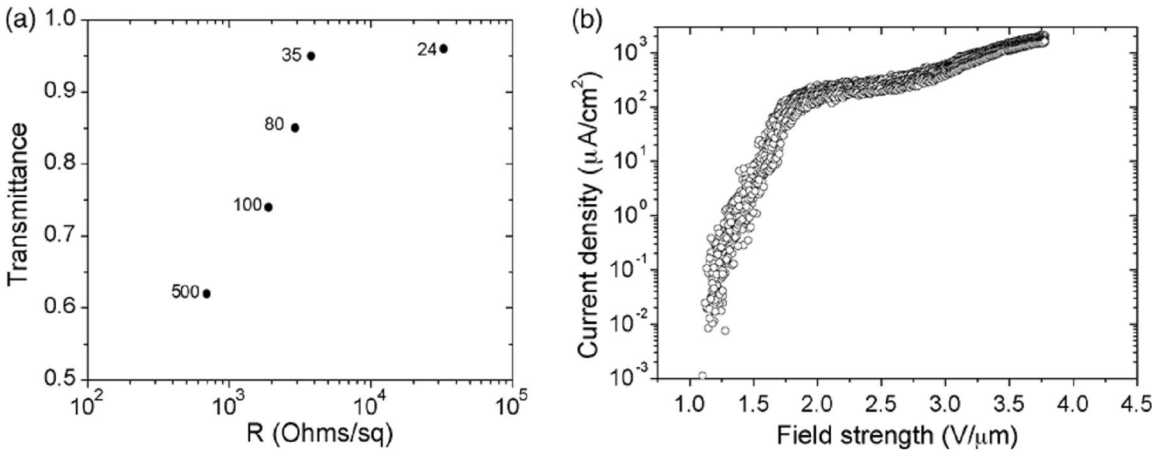

Figure 20. (a) Dependence of square resistance and transmittance (at 550 nm) on SWCNT mat thickness; numbers are given in nanometers. (b) Dependence of current density on the electric field strength.

It is worth noting that the process of integrating SWCNT mats into polymer films by thermal compression did not cause significant changes in the electrical conductivity. The relationship between square resistance and optical transmittance for SWCNT mats of different thicknesses integrated into PE films is presented in Figure 20a.

Since one of the potential applications of SWCNTs is in devices based on cold electron field emission, measurements to demonstrate the applicability of SWCNT/PE films for

such purposes were carried out. Figure 20b shows the dependence of the current density on the electric field strength obtained during 10 runs. The SWCNT/PE film exhibited a low field threshold of about 1.2 V/µm. Another advantage of such films is the presence of a clear current plateau, which is valuable, for instance, in flat-screen displays. Here, variation of the electric field between 1.7 and 2.7 V/µm did not lead to a significant change in the electron emission.

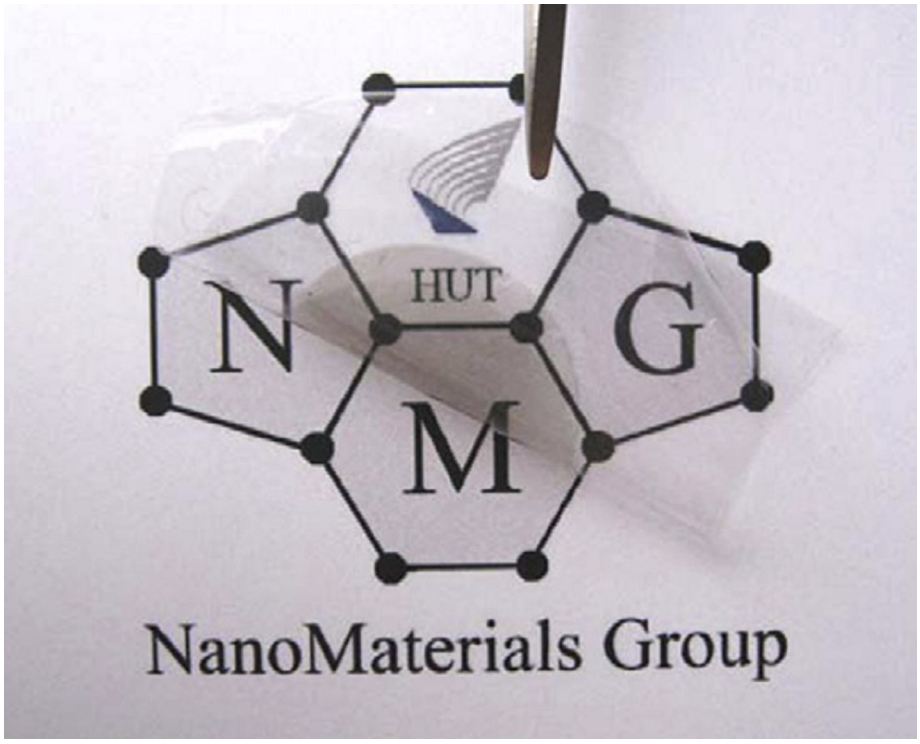

Figure 21. Illustration of the flexibility and transparency of a PE/SWCNT film produced according to the described method.

Another important and useful property of our SWCNT/PE films is their flexibility. The SWCNT/PE films were found to be bendable and could be repeatedly rolled and unrolled while retaining their transparency, conductivity, and field emission properties (Figure 21).

Nanobuds provide interesting materials for cold electron field emission due to the large number of highly curved fullerene surfaces acting as emission sites on conductive SWCNTs. A comparison of the field emissions from unaligned in-plane deposited mats

(with thicknesses between 0.5 and 1 μm) of nanobuds and equivalent mats of SWCNTs synthesized under similar conditions but without adding H_2O vapour showed that the nanobuds exhibited a lower field threshold of about 0.65 V/μm and a much higher current density compared with those of pure SWCNTs (Figure 22).

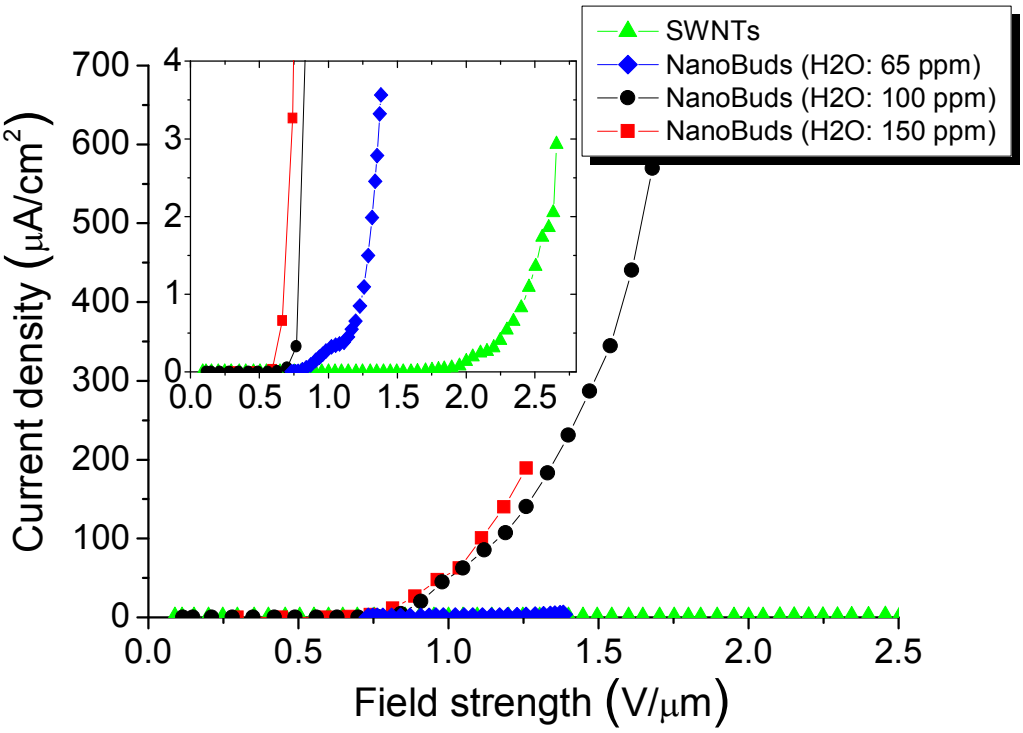

Figure 22. Field-emission properties of nanobuds. Comparison of averaged current density versus electric field strength of nanobuds (synthesized in a ferrocene reactor in the presence of 65, 100, and 150 ppm of added water vapour) with that of a sample of SWCNTs (synthesized without added water vapour). Inset shows a close-up in the vicinity of the threshold voltage. Coverage of SWCNTs by fullerenes increases with water vapour concentration, resulting in higher emission current.

5 Summary

SWCNTs and nanobuds have been synthesized by CO disproportionation on the surface of iron particles produced by two different aerosol methods: hot-wire generator and ferrocene vapour decomposition.

In situ sampling investigations of the SWCNT formation by CO disproportionation reaction on Fe catalyst particles formed by ferrocene vapour decomposition have been presented. The kinetics of the SWCNT growth has been studied on the basis of *in situ* sampling from different locations in the reactor. At temperatures of 804, 836, 851, and 915 °C, the average growth rates were found to be 0.67, 1.11, 1.01, and 2.70 μm/s, respectively. The average growth rate constant complies with the Arrhenius dependence of $k = k_o \exp(-E_a/RT)$, with the pre-exponential coefficient k_0 = 1.99 × 10^6 μm/s and an activation energy of E_a = 1.39 eV. It can be concluded that the rate-limiting step of the SWCNT growth is the diffusion of carbon atoms in the solid iron catalyst.

A novel hybrid carbon material — SWCNTs covered by covalently bonded fullerenes — has been synthesized by a one-step continuous process in the HWG and ferrocene reactors. Fullerenes and CNTs were simultaneously formed by CO disproportionation on the surface of iron particles in the presence of H_2O and CO_2. The reactor wall temperature was varied from 800 to 1150 °C. Varying the amounts of H_2O and CO_2 introduced into the reactor at 1000 °C revealed that the optimal concentrations were between 45 and 245 ppm for H_2O and between 2000 and 6000 ppm for CO_2, when the ferrocene concentration was 8 ppm. The structural arrangement of highly curved fullerenes and SWCNTs has been shown to exhibit enhanced cold electron field emission properties.

Variation of the synthesis temperature at an introduced H_2O concentration of 145 ppm showed its significant effect on the fullerene concentration on the SWCNT surface. *In situ* sampling of the nanobuds formed at different locations in the reactor showed that fullerenes were formed together with CNTs in the temperature interval between 885 and

945 ºC. A mechanism for fullerene formation during the SWCNT growth has been proposed.

Spontaneous charging of SWCNTs synthesized by means of the aerosol method has been observed. The origin of this phenomenon can be directly linked to the bundling of the SWCNTs. Furthermore, on the basis of the charging phenomena, a novel method for separating bundled and individual SWCNTs synthesized using the HWG method, and for collecting the individuals on any type of solid substrate, including low-temperature ones, has been developed.

On-line DMA measurements of SWCNTs synthesized by ferrocene vapour decomposition in a CO atmosphere revealed the formation of positively and negatively charged (up to 99%) SWCNT bundles. Tandem DMA measurements showed non-equilibrium charging of the SWCNT bundles with 1–5 elementary charges. Based on the analysis of LDI-TOF experimental data, it was proposed that the positive charging of CNTs occurs because of electron emissions, while negative charging is caused by the emission of impurities from the surface of the CNTs. The charging phenomenon of CNTs can be explained in the framework of aggregation processes leading to energy release owing to minimization of the surface energy and the emission of electrons and positive adsorbed molecules.

In addition, a simple and efficient one-step integration process for transferring SWCNT mats into PE thin films has been demonstrated. These SWCNT/PE thin films exhibited good optical transparency and conductivity as well as high mechanical flexibility. The electrical conductivity of the SWCNT mats was significantly improved by ethanol densification. Cold electron field emission measurements from a SWCNT/PE film showed a low field threshold and revealed the presence of a clear current plateau at electric field strengths between 1.7 and 2.7 V/μm.

6 References

1. Iijima, S. Nature 1991; 354: 56-8.
2. Iijima, S., Ichihashi, T. Nature 1993; 363: 603-5.
3. Bethune, D.S., Kiang, C.H., de Vries, M.S., Gorman, G., Savoy, R., Vazquez, J., Beyers, R. Nature 1993; 363: 605-7.
4. Ebbesen, T.W., Ajayan, P. M. Nature 1992; 358: 220-2.
5. Takagi, D., Homma, Y., Hibino, H., Suzuki, S., Kobayashi, Y. Nano Lett. 2006; 6: 2642-45.
6. Liu, H., Takagi D., Ohno, H., Chiashi, S., Chokan,T., Homma, Y. Appl. Phys. Exp. 2008; 1: 014001.
7. Takagi, D., Kobayashi, Y., Homma, Y. J. Am. Chem. Soc. 2009; 131: 6922-3.
8. Nasibulin, A.G., Moisala, A., Brown, D.P., Jiang, H., Kauppinen, E.I. Chem. Phys. Lett. 2005; 402: 227-32.
9. Moisala, A., Nasibulin, A.G., Brown, D.P., Jiang, H., Khriachtchev, L., Kauppinen, E.I. Chem. Eng. Sci. 2006; 61: 4393-402.
10. Dresselhaus, M.S., Dresselhaus, G., Eklund, P.C. Academic Press, San Diego, 1996; 802 pp.
11. Reich, S., Thomsen, C., Maultzsch, J. Wiley-VCH, Weinheim, 2004; 236 pp.
12. http://nanotube.korea.ac.kr/study_eng_2.html
13. Meyyappan, M. Carbon Nanotubes: science and applications. CRC Press, 2005; 289 pp.
14. Hamada, N., Sawada, S. Phys. Rev. Lett. 1992; 68: 1579-81.
15. http://scienceray.com/physics/carbon-nanotubes-and-the-space-elevator/
16. Subramoney, S. Adv. Mater 1998; 10: 1157-71.
17. Kim, K.T., Cha, S., Hong, S.H. Mater. Sci. Eng. A 2006; 430: 27-33.
18. Kanagaraj, S., Varanda, F.R., Zhil'tsova, T.V. Compos. Sci. Technol. 2007; 67: 3071-7.
19. Zavodchikova, M.Y., Kulmala, T., Nasibulin, A.G., Ermolov, V., Franssila, S., Grigoras, K., Kauppinen, E. I. Nanotech. 2009; 20: 085201-1-9.

20. Novak, J.P., Lay, M.D, Perkins, F.K. Snow, E.S. Solid-State Electron. 2004; 48: 1753-6.
21. Gruner, G. J. Mater. Chem. 2006; 16: 3533-9.
22. Nguyen, C.V., Chao, K.J., Stevens, R.M.D., Delzeit, L., Cassell, A., Han, J., Meyyappan, M. Nanotech. 2001; 12: 363-7.
23. Dai, H.J., Hafner, J.H., Rinzler, A.G.; Colbert, D.T.; Smalley, R.E. Nature 1996; 384: 147-50.
24. Ishikawa, M., Yoshimura, M., Ueda, K. Appl. Surf. Sci. 2002; 188: 456-9.
25. Wu, Z., Chen, Z., Du, X., Logan, J.M., Sippel, J., Nikolou, M., Kamaras, K., Reynolds, J.R., Tanner, D.B, Hebard, A.F., Rinzler, A.G. Science 2004; 305: 1273-6.
26. Hu, L., Gruner, G., Li, D., Kaner, R.B. Cech, J. J. Appl. Phys. 2007; 101: 016102.
27. Rinzler, A.G., Hafner, J.H., Nikolaev, P., Lou, L., Kim, S.G., Tomanek, D., Colbert D., Smalley, R.E. Science 1995; 269: 1550–3.
28. Saito Y, Nishiyama T, Kato T. Mol. Cryst. Liq. Cryst. Sci. Technol. 2002; 387: 303-10.
29. Saran, N., Parikh, K., Suh, D.-S., Muñoz E., Kolla, H., Manohar, S.K. J. Am. Chem. Soc. 2004; 126: 4462-3.
30. Yu M.F., Bradley S.F., Arepalli S., Ruoff R.S. Phys. Rev. Lett. 2000; 84: 5552-5.
31. Chatterjee, T, Mitchell, C.A., Hadjiev, V.G., Krishnamoorti, R. Adv. Mater. 2007; 19: 3850-3.
32. Berber, S., Kwon, Y.-K., Tomanek, D. Phys. Rev. Lett. 2000; 84: 4613-6.
33. Osawa, E. Kluwer Academic Publishers, Dordrecht, Boston, London, 2001.
34. Thess, A., Lee, R., Nikolaev, P., Dai, H.J., Petit, P., Robert, J., Xu, C.H., Lee, Y.H., Kim, S.G., Rinzler, A.G., Colbert, D.T., Scuseria, G.E., Tomanek, D., Fischer, J.E., Smalley, R.E. Science 1996; 273: 483-7.
35. Ebbesen, T.W., Lezec, H.J., Hiura, H., Bennett, J.W., Ghaemi, H.F., Thio, T. Nature 1996; 382: 54-6.
36. Wei, B.Q., Vajtai, R., Ajayan, P.M. Appl. Phys. Lett. 2001; 79: 1172-4.
37. Moulin, J., Woytasik, M., Grandchamp, J.-P., Dufour-Gergam, E., Bosseboeuf, A. Microsyst. Technol.2007; 13: 1553–8.

38. Martel, R., Schmidt, T., Shea, H.R., Hertel, T., Avouris, P. Appl. Phys. Lett. 1998; 73: 2447-9.
39. Baughman, R.H., Zakhidov, A.A., de Heer, W.A. Science 2002; 297: 787-92.
40. Bethune, D.S., Kiang, C.H., de Vries, M.S., Gorman, G., Savoy, R., Vazquez, J., Beyers, R. Nature 1993; 363: 605-7.
41. Guo, T., Nikolaev, P., Thess, A., Colbert, D. T. and Smalley, R. E. Chem. Phys. Lett. 1995; 243: 49-54.
42. Kim, K.S., Cota-Sanchez, G., Kingston, C.T., Imris, M., Simard, B., Soucy, G. J. Phys. D: Appl. Phys. 2007; 40: 2375-87.
43. Jung, S.H., Kim, M.R., Jeong, S.H., Kim, S.U., Lee, O.J., Lee, K.H., Suh, J.H., Park, C.K. Appl. Phys. A. Processing 2003; 76: 285-6.
44. Ando, Y., Zhao, X., Sugai, T., Kumar, M. Materials Today 2004; 22-9.
45. Guo, T., Nikolaev, P., Thess, A., Colbert, D. T., Smalley, R. E.. Chem. Phys. Lett. 1995; 243: 49-54.
46. Yudasaka, M., Yamada, R., Sensui, N., Wilkins, T., Ichihashi, T., Iijima, S.. J. Phys. Chem. B. 1999; 103: 6224-9.
47. Eklund, P.C., Pradhan, B.K., Kim, U.J., Xiong, Q., Fischer, J.E., Friedman, A.D., Holloway, B.C., Jordan, K., Smith, M.W. Nano Letters 2002; 2: 561-6.
48. Maser, W.K., Munoz, E., Benito, A.M., Martinez, M.T., de la Fuente, G.F., Maniette, Y., Anglaret, E., Sauvajol, J.L. Chem. Phys. Lett. 1998; 292: 587-93.
49. Bolshakov, A.P., Uglov, S.A., Saveliev, A.V., Konov, V.I., Gorbunov, A.A., Pompe, W., Graff, A. Diamond Relat. Mater. 2002; 11: 927-30.
50. http://www.pvd-coatings.co.uk/theory-of-pvd-coatings-pulsed-laser-ablation.htm.
51. Dai, H., Rinzler, A.G., Nikolaev, P., Thess, A., Colbert, D. T. and Smalley, R. E. Chem. Phys. Lett. 1996; 260: 471-5.
52. Bachilo, S.M., Balzano, L., Herrera, J.E., Pompeo, F., Resasco, D.E. and Weisman, R. B. J. Am. Chem. Soc. 2003; 125: 11186-7.
53. Homma, Y., Yamashita, T., Finnie, P., Tomita, M., Ogino, T. . Jpn. J. Appl. Phys., Part 2 2002; 41: L89-L91.
54. Zhou, Z., Ci, L., Chen, X., Tang, D., Yan, X., Liu, D., Liang, Y., Yuan, H., Zhou, W., Wang, G. and Xie, S. Carbon 2003; 41: 337-42.

55. Bladh, K., Falk, L.K.L., Rohmund, F. Appl. Phys. A. 2000; 70, 317-22.
56. Moisala, A., Nasibulin, A.G., Brown, D., Jiang, H., Khriachtchev, L., Kauppinen, E.I. Chem. Eng. Sci. 2006; 61: 4393–402.
57. Nikolaev, P.M., Bronikowski, J., Bradley, R.K., Rohmund, F., Colbert, D.T., Smith, K.A., Smalley, R.E. Chem. Phys. Lett. 1999; 313: 91-7.
58. Nikolaev, P. J. Nanosci. Nanotechnol. 2004; 4: 307-16.
59. Knutson, E.O., Whitby, K.T. J. Aerosol. Sci. 1975; 6: 443–51.
60. Moisala, A., Nasibulin, A.G., Shandakov, S.D., Jiang, H., Kauppinen, E.I. Carbon 2005; 43: 2066-74.
61. Nasibulin, A.G., Queipo, P., Shandakov, S.D., Brown, D.P., Jiang, H., Pikhitsa, P.V. J. Nanosci. Nanotechnol. 2006; 6: 1233-46.
62. Nasibulin, A.G., Pikhitsa, P.V., Jiang, H., Kauppinen, E.I. Carbon 2005; 43: 2251-7.
63. Shibuta, Y., Maruyama, S. Physica B. 2002; 323: 187-9.
64. Ding, F., Rosén A., Bolton, K. Chem. Phys. Lett. 2004; 393: 309-13.
65. Wiedensohler, A. J. Aerosol Sci. 1988; 19: 387-9.
66. Friedlander, S.K. Smoke, dust, and haze. Fundamentals of Aerosol Dynamics. Oxford University Press, New York, Oxford, 2000; 432 pp.
67. Schiel, A., Weber, A.P., Kasper, G. Chem. Eng. Technol. 2002; 25: 1149-51.

ISBN 978-952-60-3086-9
ISBN 978-952-60-3087-6 (PDF)
ISSN 1795-2239
ISSN 1795-4584 (PDF)